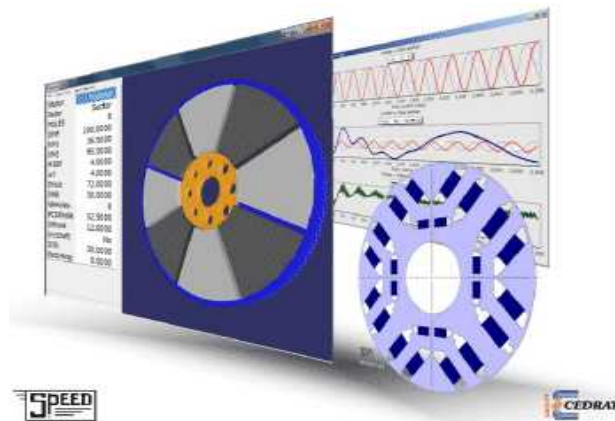
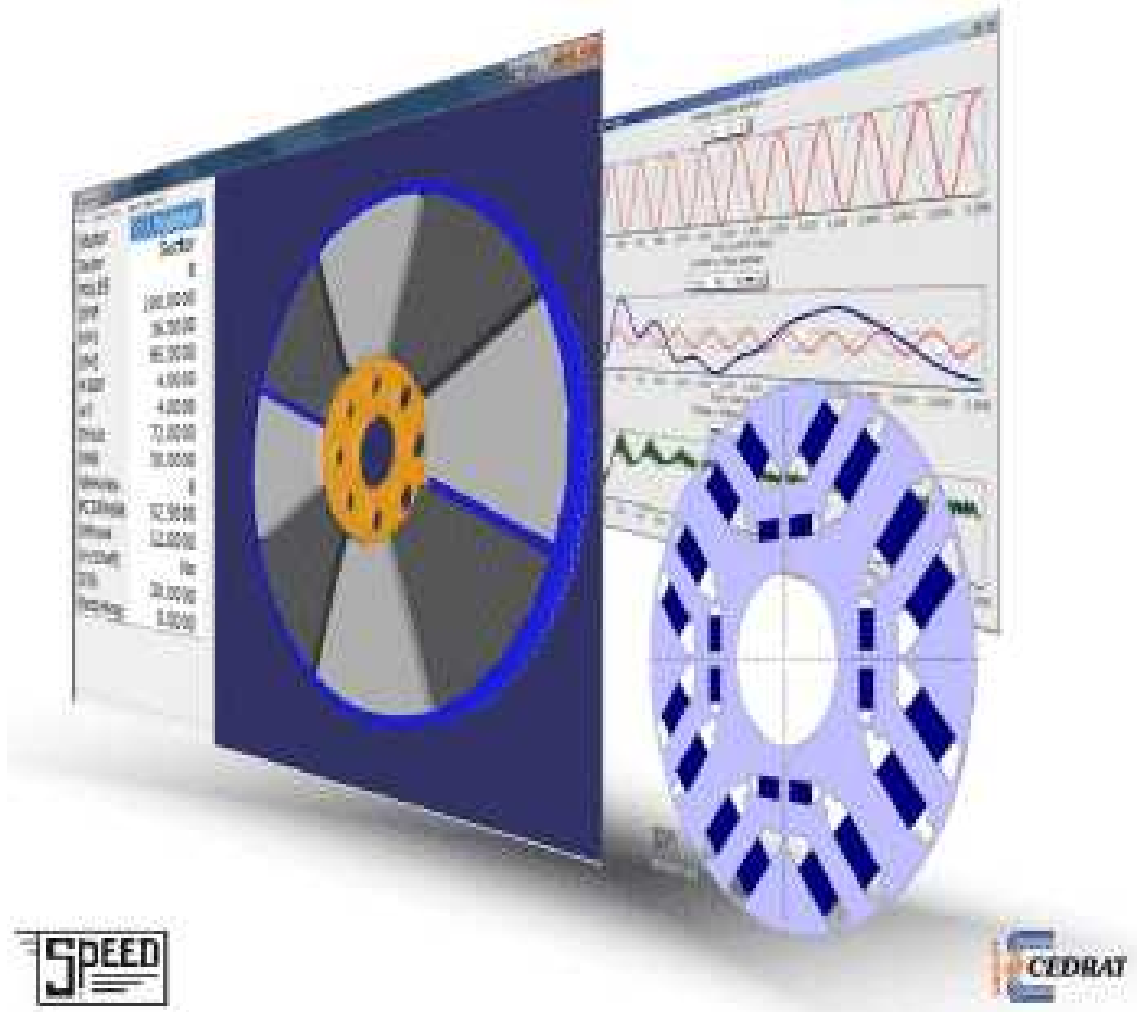


SPEED 2011

Upgrade, September 2011





What is SPEED, and what's its future?

SPEED is one of the leading design software tools for the design of electric machines. We'd like to think it is *the* leading tool. Certainly our customers are among the leading manufacturers, designers, developers and users of electric machines. We have over 1500 *SPEED* users, in all the developed countries of the world, and many of them have been using *SPEED* for over 20 years — some for as long as 25 years. Thousands of machines have been designed with *SPEED*, and millions have been produced.

The future of *SPEED* is to keep doing what it does best. There are three main ways in which *SPEED* contributes to its customers' design function:

Design of new prototypes — *SPEED* can assist a designer to prepare a new electric machine design in a very short time.

Characterization of products — *SPEED* characterizes a machine and its drive in comprehensive detail. So it is ideal for supporting the inventory of a company's designs, and it's the place to start when changes are needed.

Communication — *SPEED*'s data is highly organized in both numerical and graphical form, so it is ideal for communication between company sites, and often between supplier and customer.

Of course *SPEED* doesn't do everything. For extreme analysis of difficult electromagnetic, mechanical, or thermal problems, it works closely with high-powered specialist tools such as STAR-CCM+ for CFD, or finite-element tools. *SPEED*'s GDF geometry definition format has been widely used for porting essential data between these tools.

Changes in the *SPEED* software

Before we list the changes and new features, let's emphasize that in many ways *SPEED* hasn't changed at all. Long-term compatibility with early design files is rigorously maintained. We have taken very little out. The changes are mostly additions and corrections.

For the most part, the changes are not spectacular. They are specialized, just like the tasks that most designers are engaged on. But the changes should prove very useful to the users who need them. Almost all of them are the response to customer feedback from our technical enquiry service.

HIGHLIGHTS of SPEED — by industry

AUTOMOTIVE

including Hybrid and Electric Vehicles

Commercial, industrial, agricultural and mining special vehicles

Electrification of drivetrains and auxiliaries is a huge theme in automotive engineering, and *SPEED* is serving all sectors especially in brushless IPM and SPM machines, induction machines, switched-reluctance machines, and commutator machines and their control.

SPEED's finite-element GoFER and embedded finite-element solver combine with comprehensive analytical models covering all aspects of the design of all these machines, including thermal as well as electromagnetics and drive control.

Enhancements have been made in all aspects of these design calculations, to improve accuracy and cover an even wider range of machine geometry.

Of particular importance is the efficient utilization of magnets, and even the elimination of magnets. The *SPEED* suite of programs is now structured to give seamless design capability over the entire range of permanent-magnet machines *and* the alternatives including hybrid combinations.

SPEED covers the entire range of power, voltage, and speed used in vehicle systems.

SPEED plays a key role not only in drivetrain engineering but also in auxiliaries such as starter-generators, many kinds of pumps, blowers, and actuators, and even the KERS systems used in F1.

For auxiliary DC machines *SPEED*'s *PC-WFC* program has been enhanced with an embedded finite-element solver and many other improvements.

REFRIGERATION, DOMESTIC APPLIANCES, WATER

Efficiency requirements are driving these industries towards continual technological evolution, in a context of extreme cost pressure and material supply issues.

SPEED is used as the main design tool in several leading companies manufacturing compressors, washing-machine drive motors, pumps and fans worldwide.

The technology covers induction motors (both 1-phase and 3-phase), permanent-magnet brushless motors, and line-start PM motors. Switched reluctance motors are also used in a few key applications.

SPEED's ability to characterize *products* and not just concepts is one its main assets in serving this sector.

Improvements have been made in all programs in relation to machine geometry, loss calculations, drive control, and finite-element analysis.

AEROSPACE

High power-density, high speed and fault tolerance are key requirements in aerospace applications. *SPEED* has been used for many applications including actuators, pumps, and starter-generators, and we are "on" some of the most advanced electrically-equipped aircraft.

Brushless PM machines and switched reluctance machines are the main technologies.

In both of these areas *SPEED* has new features improving the range of machine geometry, and the calculation of electromagnetic and thermal performance.

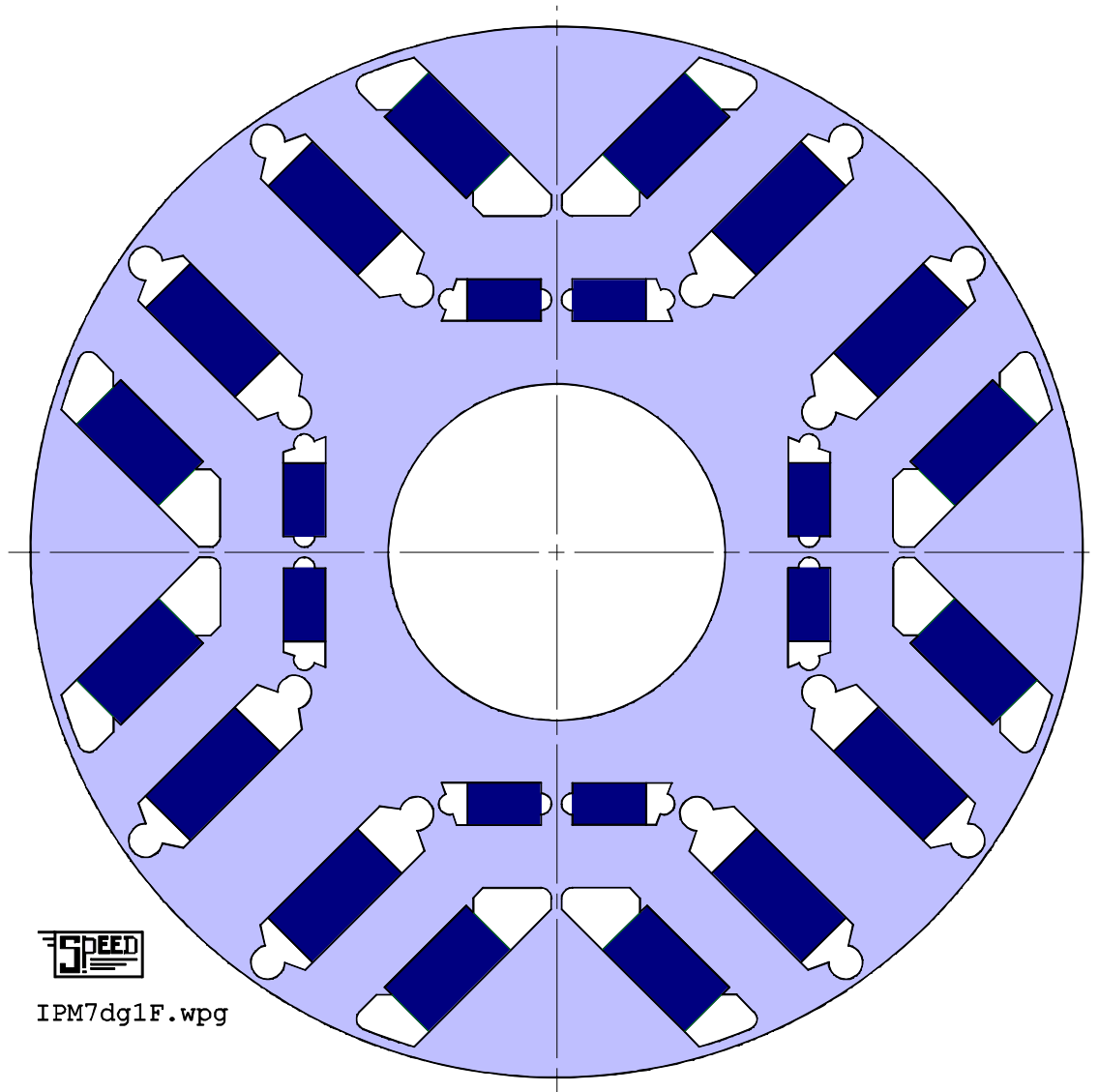
INDUSTRIAL

SPEED is behind the design of some of the world's most efficient AC variable-speed drives, using brushless SPM and IPM motor configurations. Not only in high-efficiency industrial drives, but also in precision servomotor systems.

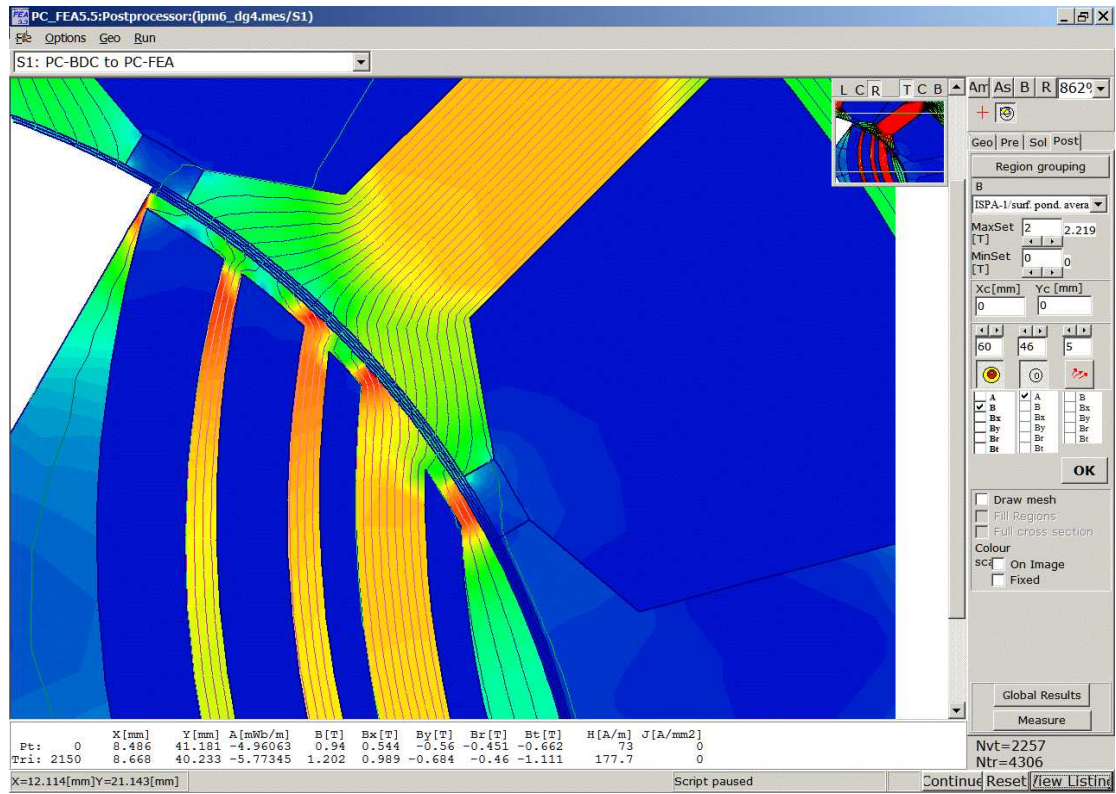
We've made special efforts to extend *SPEED* into generators, with a new embedded finite-element solver to cope with a wide variety of load specifications, and automatic calculation of generator characteristics for wound-field synchronous generators. We've added the doubly-fed induction machine to the range.

Improvements in machine geometry, finite-element analysis, drive control, and thermal modelling have been achieved. *SPEED*'s technology covers all kinds of brushless PM machines, synchronous and switched reluctance machines, induction machines and DC machines.

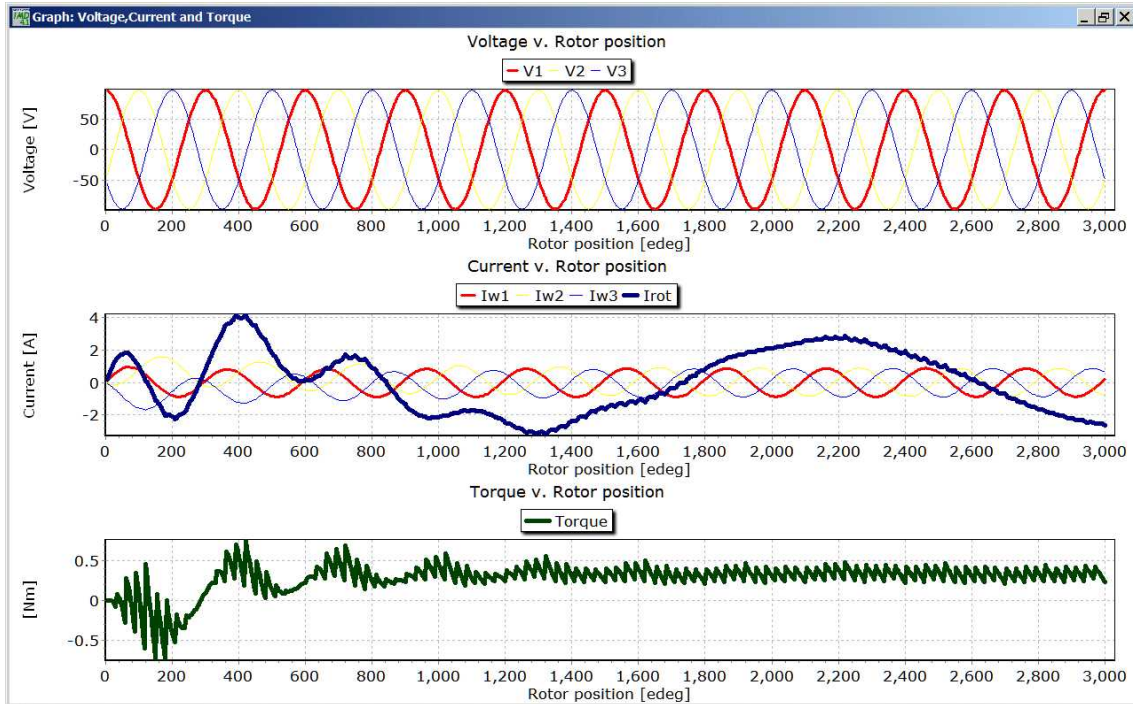
Axial-flux machines can also be calculated using a new addition to the *SPEED* system.



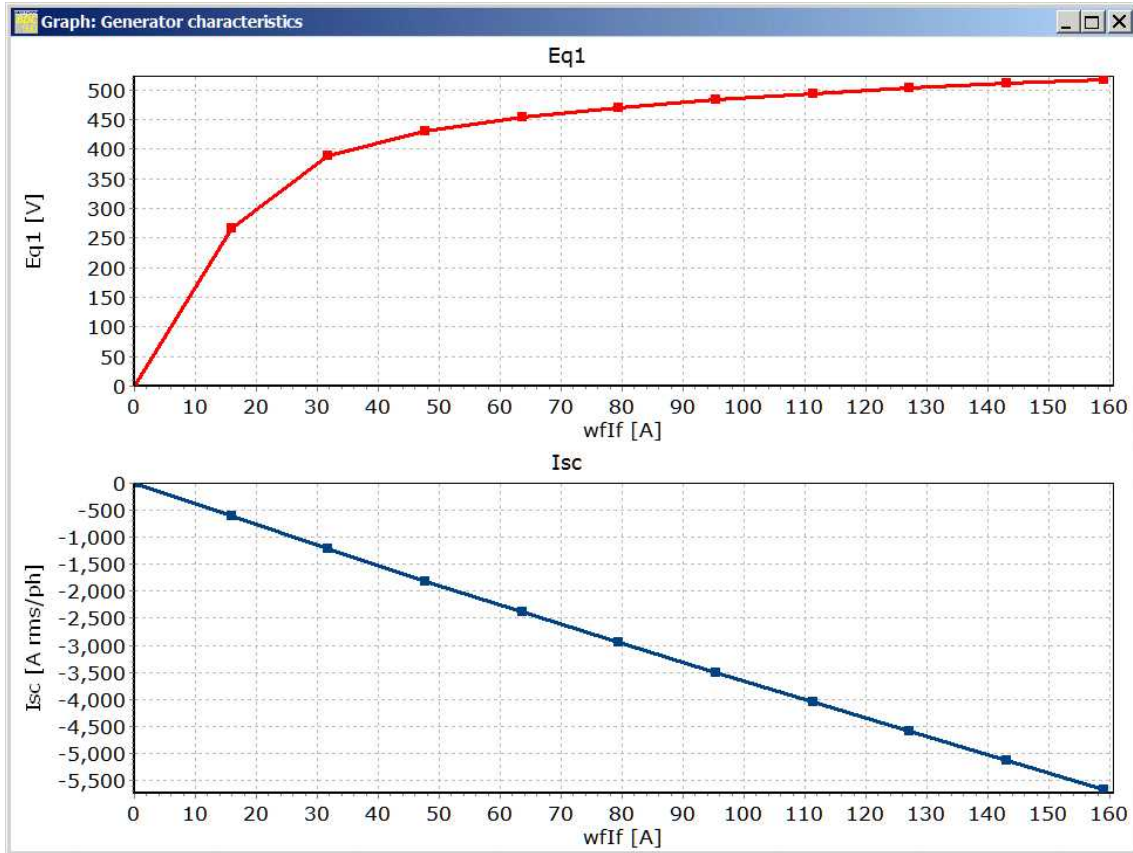
Rotor of a hybrid PM/Reluctance machine in *PC-BDC*, having a very wide range of geometric configuration options. The layers and the individual magnets can be included or excluded, and all calculations are available with *PC-BDC*'s external solvers, with the GoFER, and with the embedded finite-element solver.



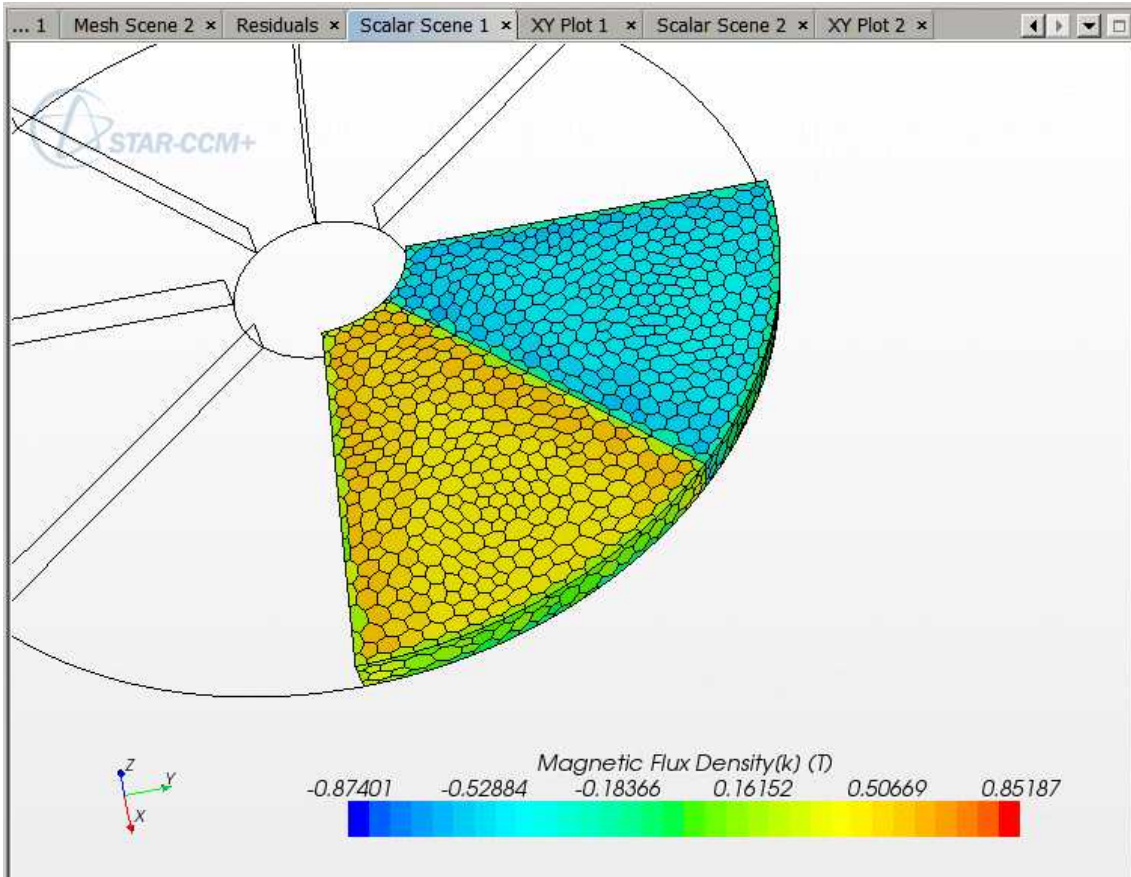
Detail of a synchronous reluctance motor in *PC-BDC/PC-FEA*, showing the multi-layer structure and the saturable bridges in the rotor. Hybrid PM/reluctance machines of this type can be fitted with magnets with a wide variety of configurations and strengths, while all of *PC-BDC*'s modelling capability can be applied to the electromagnetics, the control, and the thermal performance



Transient calculation for an induction machine in which the inductances of the stator coils and rotor bars are calculated *individually* instead of using the classical equivalent circuit. This new method avoids the simplifying assumptions made in the classical theory in relation to the effect of space harmonic effects.



Open-circuit and short-circuit characteristics of a wound-field synchronous generator, computed in *PC-BDC* automatically using a new embedded finite-element solver in about 1 minute.



Colour map of flux-densities in *STAR-CCM+* showing two magnets in an axial-flux motor modelled in *PC-AXM*. Many *SPEED* geometries can now be transferred directly to *STAR-CCM+*.

PC-BDC — Brushless DC and AC machines

1. **Synchronous reluctance machines and hybrid PM/reluctance machines** are better supported by improvements and new options in rotor geometry. For example, Fig. 2 on p. 4 shows a pure synchronous reluctance rotor with up to four flux-barriers per pole, while Fig. 3 on p. 4 shows a hybrid rotor with considerable flexibility in its configuration; (see **IPM7dg1**).

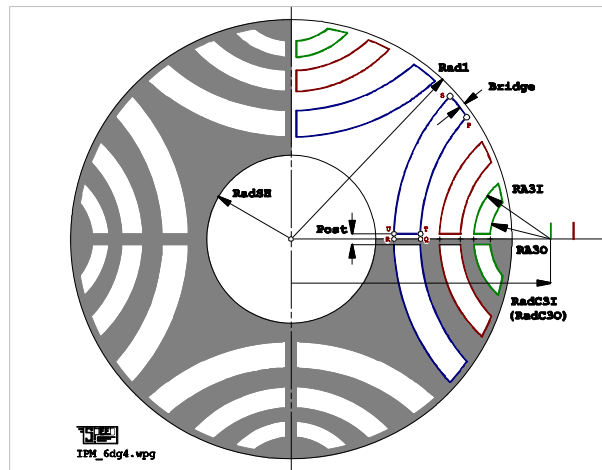


Fig. 7 **RotType** = IPM; **Embed** = Type 6;
DimGroup = Alter4

Interest in the synchronous reluctance motor is reviving because of concerns over magnet prices and availability. All the analytical power of PC-BDC / PC-FEA is available to design these machines.

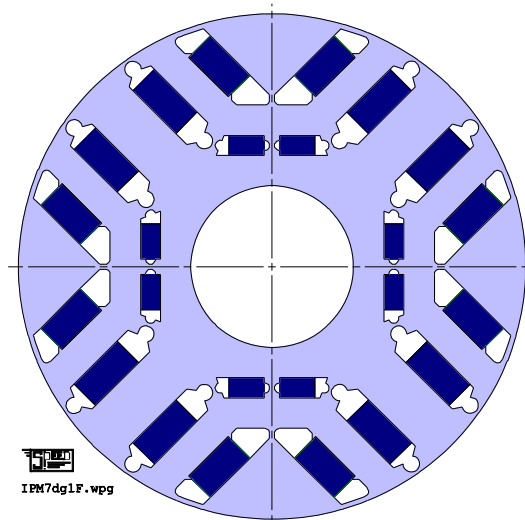


Fig. 8 **RotType** = IPM, **Embed** = Type 7;
DimGroup = Alter 1.

The hybrid PM/reluctance machine is in the hot seat of development for electric and hybrid vehicles.

2. For multi-layer IPM rotors it is now possible to “switch off” the magnets individually or all together, permitting the analysis of various options of hybrid PM/reluctance machine; (see **Magnets** and **Ly1Mag**, **Ly2Mag**, **Ly3Mag**, and **Ly4Mag**).

3. **Wound-field generators** are better supported, with several new methods of specifying the operating point; (see **LoadSpec**). Previously with **Drive** = AC Volt, the load could be specified only through **Vs** and **delta**, but **LoadSpec** provides several other options including open and short circuit, passive impedance load, and specified values of power, reactive power, and current in different combinations. For motors, the shaft torque or power can be specified.
4. A **new embedded finite-element solver** has been introduced using **PC-FEA** to work with all of the new **LoadSpec** options; (see **VDFEA**).
5. **Generator characteristics**— open-circuit EMF and short-circuit current versus field current — can be calculated automatically using the new **embedded finite-element solver**; see **VDFEA**.
6. **Superconducting rotors** can be modelled (**RotType** = WoundFld and **WFRType** = SuperCnd).
7. The calculation of **rotor eddy-current losses** in surface-magnet machines has been extended with new methods for PWM losses; (see **WMagCalc** and **HexSpec**). These methods include a harmonic-by-harmonic analysis of PWM losses that can easily be driven by an external script from harmonic test data, and a complete set of harmonics calculated for sine/triangle modulation according to a specified modulation index and carrier frequency ratio. See Tutorial B18.
8. The transient solver has been reinstated in the *i-psi* **GoFER**, but with severe restrictions and limitations explained in Tutorial B23. (Not generally available: consult the *SPEED* Laboratory).
9. **All the graphs** have been significantly upgraded with improved edit functions and **Autoscale suppression** (to prevent “jumping” after recalculation). This makes it possible to recalculate with changed parameters, without having the graph change its axis scales.
10. The **voltage locus** function in the phasor diagram has been updated to show the load point and certain other key points such as the maximum torque per ampere (optimum gamma).
11. The **phasor diagram** has been re-formatted with a tree-structure and clearer display of the numerical values. The display of individual phasors is now under the user's control.
12. The *i-psi* GoFER can now run with DC current, producing all the same outputs and files as when it runs with AC current. In particular, **static torque curves with fixed DC current** can be obtained, reflecting a commonly used test procedure in the laboratory.
13. Added **MOH1** and **MOH2** for **magnet overhang at each end of the rotor**, with completely new theoretical treatment.

PC-BDC continues its progress as a design tool for the classical wound-field synchronous machine, the workhorse of distributed generation in emergency and portable power.

Analytical estimates of rotor loss components are crucial in design and trouble-shooting, especially as the 3D eddy-current solvers are so slow and expensive to set up.

The voltage locus diagram is a crucial negotiating tool between the motor designer and the power electronics drive designer.

14. The **steel database manager** has a facility for plotting core loss vs. frequency and flux-density from the core-loss coefficients. It can also show the comparison between the losses in different materials.
15. User-defined synchronous reactance coefficients **uGd** and **uGq** have been introduced to cater for extreme geometries that are beyond the scope of *PC-BDC* to calculate, but which can still be analyzed using the **GoFER** or the embedded solver.
16. It is now possible to calculate motors with **unwound stator teeth** and what we call "**magnetically isolated slots**" (also known as "**modular**" stators): see **S_Slot** = MISlot.
17. Changes in rotor **geometry** include the addition of **Cweb**, **Edges**, **Notch**, **qFlat**, **R_qf** and **R_qff** for IPM Type1. These changes give much greater flexibility in modelling a profiled rotor surface. Also **fil_RSB** for BreadLoaf.
18. The **geometry** of the IPM with **RotType** = IPM, **Embed** = Type1 has been extended to include double magnets with a V-angle when **Vtrap** is other than 0 or 180°.
19. **Bracing bridges** have been added to **RotType** = IPM with **Embed** = NOT, giving yet another IPM geometry with possibilities for larger machines.
20. A new line-start IPM geometry has been introduced with **RotType** = Trapeze, **Embed** = Type4.
21. For **RotType** = BreadLoaf, **Embed** = Type4, **wMag** was incorrectly calculated from the coordinates of point F It has been corrected to be equal to **MagWid**.
22. The output parameter **MslotWid** (internal name #piMslotWidth) has been renamed **WmagSlot** to avoid confusion with the input **MslotWid**. **MslotWid** is one of the rotor dimensions when **RotType** = ExtPll (**Embed** = Type3 only); IPM (**Embed** = Not, Type1, Type2); and Trapeze (**Embed** = Type4). **WmagSlot** is now used only to estimate the width of the magnet aperture in the lamination when calculating **prl** (q.v.). In cases where it is not so used, **WmagSlot** = 0.
23. **WireCR**, **WireCR2**, **WireCRA** and **wfWireCR** introduced (corner-radius on rectangular magnet wire). When importing old files, check that **WireCR** = 0 and likewise with the other corner-radii if the other wires are being used. [10-Oct-09]
24. For **S_Slot** = PllSlot there is a very small correction to the slot perimeter **SlotPeri** and the surface area of one slot-liner, **SSArea**. [Corrected 9-Oct-09]
25. Two small corrections have been made in the geometry of the stator slot **S_Slot** = HW, **SlotBot** = PolyBot.
26. The IPM with **RotType** = IPM, **Embed** = Type3 has a new variant with constant magnet length (in the direction of magnetization) and a profiled rotor surface.
27. **wfMLT** has been corrected with the addition of **Shim**, and the length around the "elbows", so the field resistance **Rf** and the copper weight **wfWt_Cu** both change.
28. A Variant of **S_Slot** = GolfTee with **Rake** and **C_TH** allows "crowned teeth" on the stator.
29. **RotType** = Spoke, **Embed** = Type 3 added.

Steel characterization becomes ever more important, and SPEED's database manager provides easy-to-use organization and data conditioning.

30. Option **LamAlign** to align a non-circular lamination outline with a slot axis or a tooth axis.
31. Added **LamShape** = CoolRing geometry, permitting arrays of cooling holes in large machines.
32. **ToothSock** with parameters **SockOffs**, **SockArc**, **SockRad**, **SockAng**, **SockLeg**, **NSockLeg**, **NSockArc**. This is a contour that works with i-psi GoFER. The contour is visible in the OUTLINE EDITOR and the GDF EDITOR. The output in *PC-FEA* is a file containing (x,y) co-ordinates and the radial and tangential flux-density B (measured from the origin). These are intended for further processing (for example, in estimating force distributions by Maxwell stress), but at present there is no further processing.
33. The calculation of the multi-layer IPM (**RotType** = IPM, **Embed** = Type6) has been rewritten to correct a minor error in which changes in the geometry of deactivated magnets could still affect the result. Corrections also in the GoFER for the case of **Magnets** = None.
34. **Lstk** has been added to the TEMPLATE EDITOR.
35. Introduced **WstCalc** to resolve differences between the effective tooth width used by the finite-element **GoFER** and *PC-BDC* itself, particularly when a non-zero value of **filSO** was being used.
36. If **WstCalc** = New or FEA, an error in the calculation of **EffWst** is corrected. This caused discrepancies between *PC-BDC* and the B_{tooth} **GoFER**. Upgraded files with adjustment factors based on **MatchFE** | **Btooth** should be re-calibrated. Also see **WstCalc**.
37. **S_Slot** = OneOHang added; this is an asymmetrical stator slot used with form-wound coils.
38. **RSWdg** added; radius at which B_{gap} is calculated when **EMFCalc** = HBMethod or KFR.
39. Bracing bridge **wBB** and centre web **CWeb** have been added to **RotType** = IPM, **Embed** = Type5.
40. Slot wedge (**SSWedge**, **WSWedge**) added to **S_Slot** = PllTooth.
41. **Subtransient reactance and time-constant** are calculated for both surface-magnet and interior-magnet machines.
42. **Symmetrical 3-phase short-circuit faults** can be calculated using **Analysis** | **Short circuit**. This includes all subtransient effects and DC offset.
43. **Torque transients** can be calculated dynamically using **Analysis** | **Torque transient**.
44. The **Fourier Transform** is used to estimate the flux-density in the magnet during short-circuit faults and torque transients.
45. The **field due to individual winding space-harmonics** and **individual time-harmonics** in the current waveform can be calculated in isolation for surface-magnet machines.
46. A **screening function** can be calculated for rotor cans or screening cylinders.

47. The **slot-ripple** in the B_{gap} distribution has been significantly improved with a new method **SlotMod = HH**. This brings a marked and automatic improvement in the calculation of cogging torque and rotor eddy-current loss.
48. **Multiplex windings** can be modelled in **Static design** with **Drive = Sine** or **AC Volt**, with new **Connex** options 4-phase, 6-phase, and 9-phase. See **Connex**, **Plex**, and **PolyOffs**.
49. The **embedded finite-element solver (ipsiCalc = PCFEA)** for sinewave machines provides automatic adjustment of **Xd**, **Xq**, and **Eq1** to match the finite-element values. This process has been made more robust and faster. This very important modification is selected with **MatchFES**; It bypasses the *i-psi* **GoFER** so that the process of determining saturation factors is both *automatic* and *unique*. This will improve productivity when designing highly saturated IPM machines.
50. **PC-BDC** admits different values for the differential leakage reactance in the *d*- and *q*-axes; (see **Xdiff_d** and **Xdiff_q**). When using the embedded finite-element solver with **MatchFES**, this resolves a serious difficulty in obtaining unique saturation factors, especially in machines with significant differential leakage. The result is a marked improvement in the quality and consistency of the results for saturated machines, with a reduction in labour.
51. The **MatchFES** facility with the embedded finite-element solver has been extended to cover wound-field machines; instead of adjusting **XBrT** for the magnet remanence, it adjusts **XIf** for the effective field current.
52. **Magnet flux pulsation** due to slotting and winding harmonics can now be calculated using the *i-psi* **GoFER**. (See **FPLoss**, **NPHx**, **PhiMn**, **nPhiMn**, **R_FP** and **Beta_FP**).
53. **Direct torque control** has been added as an option of **Sw_Ctl** with **Drive = Sine**.
54. There is now have a **wider selection of methods for controlling the carrier frequency and switching frequency** of the various current-regulators, through two new options of **FixfChop**, **UCFR** and **ISChop12**.
55. We can now control the **carrier frequency for squarewave drives** as well as sinewave drives. When **Drive = Square** and **Sw_Ctl = C120_Q1**, **C60_Q1**, etc., the sampling rate **f0** at which the current waveform is compared with the hysteresis band can be controlled *via* **FixfChop**. Previously, this comparison was made at every integration step, implying a sampling rate of $720 \times \text{ISLA} * \text{Freq1}$. This value is retained if **FixfChop = No**.

56. Significant improvements have been made to the **sine-triangle modulator** used with the ramp-comparison current regulator, the synchronous regulator, and the sine/triangle voltage PWM modulator (**Sw_Ctl** = RampComp, SynchReg, and VPWM_ST). The switching frequency is more robustly controlled and the integral gain function is greatly improved. In earlier versions there was a problem in that the switching frequency increased in the overmodulation range, when it should have decreased; this has been fixed.
57. The **Hot10 thermal model** has been extended to **exterior-rotor motors** with **RotType** = ExtRad or ExtPll.
58. The calculation of the thermal resistance **R_ts** has been reworked in the Hot10 thermal model, updating it to allow for details in slot geometry, with various corrections.
59. The Hot10 thermal model now has additional **heat-transfer paths for the end-windings**, represented by **ThR_EA** and **EndCool**. This makes it easier to simulate motors with **direct air-cooling of the end-windings**.
60. The Hot10 thermal model now has two additional infinite heat sinks, the U and V nodes, so that convection and conduction can be "connected" to **heat-sinks at different temperatures**. This is convenient for machines mounted on hot (or cold) surfaces which are not at ambient temperature.
61. **Single-phase motors fed from AC voltage source**. *PC-BDC* now calculates the steady-state **static design** for split-phase capacitor motors and pure single-phase motors, even when there is no rotor cage. Although these motors are not self-starting, the **Analysis | Line-start** calculation can be used to study load-perturbation transients in these motors. The phasor diagram for split-phase and line-start motors has been greatly improved and **SEM-2** has a thorough description of the theory. **UserLS** and **fs** have been removed. **SymmCpts**, **RPMstart**, **ConstRPM** and **AngOn** have been introduced, and **LoadStep** has changed its function slightly. **VLpp** and **VLph** have been introduced. **AuxSpec** has been extended with the SinglePh option. See entries for these parameters.
62. *PC-BDC* can now model **single-phase generators** working with **Drive** = AC Volt, **Connex** = 1-ph, **Sw_Ctl** = Generator, together with appropriate settings of **SymmCpts** and **AuxSpec**. This includes machines with auxiliary capacitor windings and salient-pole rotors.
63. The **Dynamic design** calculation for **Drive** = AC Volt has been revised, so that much better agreement should be obtained between **Static design** and **Dynamic design**, for all cases where **Drive** = AC Volt, with **Connex** = Wye or Delta, and **Sw_Ctl** = Motor or Generator. In versions before 7.6.0.8.E, 16-Jul-07, **Dynamic design** was merely being used to display sinusoidal waveforms of current and voltage with phase angles determined from **Static design**.
64. The switching loss **WSwitch** has been revised and corrected, and the number of switching cycles (**NccQ1**) is displayed, so that **WSwitch** and the switching frequency **SwFreq** can be checked by manual calculations.
65. New parameters **Vct1** and **Vht1** have been added, to define certain maximum available voltages under PWM control.

66. All **Rectifier** calculations can now be made with **DCSource** = Fixed DC or DC Filter. "Fixed DC" provides a simpler set-up, although it may be necessary to ensure sufficient circuit resistance to get satisfactory damping (i.e., attenuation of the initial DC offset transient). See **Drive** and **DCSource**.
67. Several corrections and improvements have been made in calculations with **Drive** = Rectifier, including the related cases of "Over-running" when **Drive** = Square or Sine, which can sometimes be used to check the Rectifier calculations.
68. The **slot-permeance coefficient** can be adjusted by **XPCslot**; and by **XPCslotM** when calculating mutual inductance between coil-sides sharing the same slot.
69. A new **low-speed regenerating mode** based on the principle of the up-converter or step-up chopper has been added, with **ChopType** = UPG and **Drive** = Square. It works only with **Connex** = Wye.
70. For **RotType** = IPM, **Embed** = Type1, the magnet weight and inertia were incorrectly calculated in cases with *inclined magnets* (i.e., when **Edges** = Squared or Rounded and **Vtrap** not equal to 0 or 180°). Also for this rotor type, the leakage in **CWeb** was not accounted for; **pri** was incorrect [both corrected 15-Feb-10]; and **RYoke** was also incorrect [corrected 30-Jul-09]. These errors could significantly affect the magnet and rotor weights and inertias as well as the magnetic circuit calculation. To *revert* a calculation to the previous version(s), tests can be applied using the following parameter values (but do not *retain* these values after testing): **bBsat** = 10^{-12} to eliminate bridge leakage and nullify the effect of the omission of **CWeb**; **Xri** = 10^{-12} to nullify the error in **pri**; and **XRYoke** = 10^6 to force **Bry** to a small value, removing its influence from the magnetic circuit calculation. Instead of changing **XRYoke**, set **XLry** = 10^{-12} to remove the MMF drop in the rotor yoke from the magnetic circuit calculation.
71. For versions compiled between 9-Nov-09 and 15-Feb-10, when **Skew** ≠ 0 and **EMFCalc** = ToothFlux, the EMF waveform was phase-shifted, producing an error in the torque and other performance calculations. This is fixed.
72. A small phase-shift (< 0.5°) introduced in the displayed EMF waveform after **Dynamic design** with **Drive** = Sine has been corrected. The correction is applied if **CalcVer** > cv9.
73. A spurious phase-shift in the EMF waveform introduced when **EMFCalc** = ExtTFW or ExtEMF and **Skew** ≠ 0 has been corrected.
74. An error in the calculation of the rotor leakage permeance **pri** has been corrected for **RotType** = Spoke. Machines with very large rotor diameter and a large number of poles would have an excessively large value of **pri**. This would appear as an abnormally low EMF.
75. Several magnetic parameters have been corrected for the wound-field rotor with **WFRTType** = CylRotor, including **BgOC**, **Bg1**, **BgAvOC**, and the B_{gap} distribution. Much better agreement with the B_{gap} **GoFER** is obtained as a result.
76. Also for the wound-field rotor with **WFRTType** = CylRotor, a saturable element has been added in the magnetic circuit for the main pole section (lying between the innermost slots of each pole). It uses the "cc" section and produces the flux-density **Bcc** in the **design sheet**. **XLcc** is used to adjust the effective magnetic length of this section; (by default, this length is set to **SD_R1/3**).

77. For the wound-field rotor with **WFRType** = CylRotor, the axial length of the rotor (effective in the magnetic circuit) is **wfLPole**. Formerly this was greyed-out in the **template editor**.
78. With multiplex windings **Connex** = 6-phase and 9-phase, and **Drive** = Sine, the value of **VLL1** in the **design sheet** was displayed too low by a factor $\sqrt{3}$. As this parameter was not used in calculations, the error is isolated.
79. With multiplex windings **Connex** = 6-phase and 9-phase, and **Drive** = AC Volt, the input voltages **Vs**, **Vs2** and **Vs3** were not being divided by $\sqrt{3}$ to get the phase voltages. This error could be worked round by premultiplying **Vs**, **Vs2** (and if **Connex** = 9-phase also **Vs3**) by $\sqrt{3}$.
80. With multiplex windings **Connex** = 4-phase, and **Drive** = AC Volt, **Vs** was being incorrectly divided by $\sqrt{3}$ to drive the first multiplex set, but not **Vs2**. This error could be worked round by premultiplying **Vs** by $\sqrt{3}$, but not **Vs2**. This is no longer necessary.
81. With **RotType** = LSIPM or Trapeze, **ISPBal** was being calculated incorrectly as **Imain/beta** instead of **I1/beta**.
82. **XQWeb** has been added to make fine adjustments to the effective magnetic width of the *q*-axis web for **RotType** = IPM, LSIPM and Trapeze.
83. An error has been fixed in the conversion of inertia units in all conversions involving lb-ft² units (that is, the mass-based definition of inertia also recognized as *Mk*² or mass times radius of gyration squared, in English units). The error was a missing factor of 12.
84. **Rac** and **Lac** are now active for STATIC DESIGN when **Drive** = Sine, permitting the effect of series impedance (such as cable impedance) to be calculated and displayed in the phasor diagram and the DESIGN SHEET.
85. When **Drive** = AC Volt, **SPF** is more clearly identified as the power-factor at the terminals of the "Vs" source, to distinguish it from the power-factor **PF** at the terminals of the machine. Likewise when **Drive** = Sine, **SPF** is the power factor at the terminals of the inverter. If **Rac** = **Lac** = 0, then **SPF** = **PF**. Note that **SPF** = cos(**phiS**) and PF = cos(**phi**).
86. Fixed a problem with the convergence calculation in DYNAMIC DESIGN when **Drive** = Square and **dq0** = true.
87. When **RotType** = WoundFld, **Bst** and **Bsy** were displayed with incorrect values in the design sheet.
88. The usage of **XSpan** has changed, so that it now works with **CalcLdLq** = Laplace. Furthermore, if **CalcLdLq** = Lumped, **XSpan** works only with **CalcLg** = LgMeth3. Previously it worked only with **CalcLg** = LgMeth1.
89. When **BalWdg** = false, any winding having **TC** > 178 (or any coil with more than 178 turns) may have a negative calculated value of **Lslot** in earlier versions.

90. The SynchReg and SVMModX current-regulators now work for delta-connected motors as well as wye-connected motors.
91. **FEshow** can be used to display the operation of the embedded finite-element solver briefly during execution, as a diagnostic tool in case of problems.
92. The warning message "current is leaking outside hysteresis band" no longer appears unless **Sw_Ctl** = ISP_HB. Note that this message appears only if the current leaks outside a hysteresis band equal to twice the width of the normal hysteresis band **ISP/HBA**.
93. **Connex** = "Delta" is now displayed instead of "Open delta". Before 2003, the simulation equations for the delta connection with **Drive** = Sine did not allow circulating current in the delta. These equations were modified in Dec. 2003 with the addition of **Rac** and **Lac**, but the annunciation was not updated. This item is relevant only if you have files created with **Drive** = Sine before December 2003, and then only if you have a concern with zero-sequence circulating current in the delta; the earlier versions did not recognize it, but the subsequent versions do.
94. An error introduced in the Hot10 thermal model at 10-Oct-07 has been fixed. This error caused complete failure of the Hot10 model, and the symptoms would be immediately recognizable in the transient thermal graphs.
95. Fixed an error in the graphical display of second half-cycle of current waveforms.
96. Removed various error conditions arising when **Vs** = 0 with **Drive** = AC Volt. It is now possible to run a short-circuit calculation (as in Tutorial B16, *Generators and Rectifiers*).
97. Introduced "rectified EMF" parameters **ErecAv** and **ErecRMS**.
98. Introduced waveform of line-line rectified open-circuit EMF, displayed with the DC voltage waveforms when **DCSource** = DCFilter or **Drive** = Rectifier.
99. Corrected several errors in the determination of **OpMode** (Motoring or Generating) when **Drive** = AC Volt. The symptoms of these errors were variously as follows :
 - (a) **Pelec** would not agree with $\sqrt{3} \times \mathbf{Vs} * \mathbf{ILrms} * \mathbf{PF}$ after **Static design**, (or the equivalent formula for 1-phase or 2-phase cases).
 - (b) One or more of the component torques **Tei**, **Trel** (for **Dynamic design**) or **TEI_PS**, **Trel_PS** (for **Static design**) would have the wrong sign.
 - (c) **OpMode** would have the wrong value.
100. If **Drive** = Square and **Sw_Ctl** = V60_Q6, V120_Q1, V90_Q1 or V180_Q1, the current-limit at **ISP** now has a latching function so that the limiting action is by chopping at the frequency **f0** (q.v.) and not at an uncontrolled frequency. The switching frequency **SwFreq** is correctly calculated to reflect this condition, and the switching loss **WSwitch**.
101. If **Drive** = Square and **Connex** = 3-ph Uni, the blocking diode can be removed if **UBkDiode** = false, or retained if **UBkDiode** = true.

102. Additional new parameters **Psi1rms** and **phPsi1**. (q.v.)
103. Added **PCWire**, **TCCWire** and **WireDens** to permit materials other than copper to be used for stator windings.
104. An error has been fixed in the calculation of inertia **RotJ** and rotor iron weight **wt_FeR** for **RotType** = IPM, **Embed** = Type1, when **R_rpf** \neq 0, i.e., rotors with a profiled surface. The error manifested itself as a large and incorrect reduction in inertia.
105. Rectifier current waveforms are now displayed with the "positive generating current" convention. Compared with earlier versions, the current waveform will appear to be reversed.
106. As part of the aforementioned improvement in **Dynamic design** with **Drive** = AC Volt, corrections have been made to the phase angles of the fundamental current, EMF, and phase voltage. The fundamental phase voltage is reconstructed after the **Dynamic design** calculation using a method determined by **CalcVwfm**. The relevant phase angles are **phV1**, **phI1**, and the difference between them **phi_1**, which is the fundamental power-factor angle. These angles should now be consistent with the phase angles appearing in the phasor diagram. The agreement will not be exact, because the phasor diagram is calculated in **Static design**, whereas the "reconstructed" angles **phV1** and **phI1** are the result of a large amount of number-crunching (with arrays of limited resolution, in the interest of speedy calculation). However, they serve to check the correctness of both the **Static design** and **Dynamic design** calculations. Note that the relevant fundamental RMS voltages and currents reconstructed from **Dynamic design** are **V1rms** and **I1rms**, with components **V1d**, **V1q**, and **I1d**, **I1q**. (The corresponding **Static design** components are **Vd1**, **Vq1**, **Id1** and **Iq1**).
107. An error has been fixed in the rotor weight (**wt_FeR**) and inertia (**RotJ**) of line-start motors (**RotType** = Trapeze or LSIPM). Also, when **Embed** = Type2 or Type 3, these parameters could vary on successive calculations. In known cases the error is very small (<2% in both **wt_FeR** and **RotJ**). A different but related correction results in an even smaller change in **R_2d** and **R_2q**, of the order of less than 0.01%.
108. An error has been fixed in the calculation of **Lgg** and **Mgg** in cases where the three methods of **CalcLg** gave different results, notably where a negative value of **Offset** was being used.
109. The iron loss can now be rescaled according to the airgap flux-density calculated with **Drive** = Sine as well as **Drive** = AC Volt, and this rescaling has been made optional; see **WFeScale**.
110. **Id_Min** and **Iq_min** have been introduced to define the smallest values of current I_d or I_q at which the embedded solver attempts to calculate **Ld_FES** and **Lq_FES**.
111. Versions released with the embedded FE solver before version 8.0 may have omitted the end-turn inductance **Lendt** and the "extra" inductance **Lext** when updating **Ld** and **Lq** from the finite-element values **Ld_FES** and **Lq_FES** (or **Ld_FE** and **Lq_FE**) following a **Static design** or **Dynamic design**. This could be detected by changing **XLendt** (say, from 1 to 0) and observing no change in **Ld**, **Lq**, **Xd** or **Xq**. Torque calculations are not affected by this error.

112. A spurious ripple in the EMF waveform could appear when **EMFCalc** = ToothFlux and **BTSR** = true, especially with a small number of slots/pole. This can be overcome by setting the new parameter **NBTSR** to a higher value.
113. A cubic-spline interpolation of the B_{gap} waveform has been introduced to complement the linear interpolation obtained previously with **BTSR** = true.
114. The diagram explaining the structure of *PC-BDC*'s inductance parameters has been simplified and corrected.
115. "Cross-coupling" gain coefficients **G_dq** and **G_qd** have been added for the SynchReg and SVMdX current-regulators.
116. **SolvMG** has been added to activate the gain describing function of Rowan and Kerkman when **Sw_Ctl** = SynchReg. See Tutorial B09.
117. An error has been fixed in the equations for V_{dm} and V_{qm} . $R_{ph}I_{dm}$ and $R_{ph}I_{qm}$ were interchanged.
118. Third-harmonic injection has been added for **Sw_Ctl** = VPWM_ST and SynchReg; see **MIX3** and Tutorial B09.
119. **XdGap** introduced to adjust the magnetic effect of **dGap**.
120. **ShellFlux** has been renamed **ShAxFlux**, and at the same time, its usage has been corrected; see **SEM-2**.
121. A missing half of the Lissajous figure for space-vectors when **Sw_Ctl** = SynchReg or SVMdX has been restored.
122. The error messages for "Carrier frequency f0 is too low" and "Carrier frequency f0 is too high" have been changed to warnings.
123. A correction has been made in the SynchReg current regulator (**Sw_Ctl**), so that the phase of the model-reference feedforward signal is consistent with the rotor coordinate system. A new tutorial B20 has been written to provide an example of the SynchReg regulator.
124. **ISPSpec** has been added so that the set-point current can be specified as a peak or RMS value; or in terms of cartesian components **ISPd** and **ISPq**.
125. A small error in the direction of magnetization in the IPM Type 4 rotor has been corrected. This error existed only when **Inset** was non-zero.
126. Added **t_FS**, **t_FC** to control the timing of short-circuit faults, and **Prefault** to select the pre-fault operating condition.
127. Added **t_TS**, **t_TC** to control the timing of torque steps.
128. When **EMFCalc** = HBMethod, the skew factor was being applied as though **Skew** were $2 \times \text{Skew}$. This has been fixed.
129. The polarity of the tangential magnetization was reversed when **EMFCalc** = KFR and **MagType** = Sine or Halbach.
130. The internal magnetic equivalent-circuit solver (used with **EMFCalc** = BLV, ToothFlux) now displays a warning if the flux-density in any section exceeds 2.2 T.

131. **XBetaM** is now active for adjusting the effective magnetic value of **BetaM** for those geometries that use **BetaM**. This will have some benefit in making adjustments using **MatchFE**.
132. **Connex** = 5-phase has been removed. It should not have been in the list because it was never developed.
133. An error has been fixed in the calculation of **HkT**. The temperature coefficient **CHcJ** was previously being applied with the wrong sign.
134. The **SPEED kT Calculator (Tools | kT,kE)** has been added to provide a comprehensive calculation of the torque constant k_T , taking into account all the common methods of definition, the mixing of EMF and current waveforms, and all common systems of units.

An essential tool for matching servo-motors to the drive
135. In **Tools | kT,kE**, the motor constant K_m is calculated. This parameter is not displayed in the **PC-BDC design sheet**.
136. In **Tools | kT,kE**, the results were originally incorrect for all units other than Nm. This is fixed.
137. An **imbalance calculator** has been added to show the relationship between sequence components and different types of imbalance in 3-phase machines. (**Analysis | Imbalance**).
138. A **tooth force calculator** has been added to show the changing radial force on stator teeth as the rotor rotates. (**Results | B squared**).
139. The **Tutorials** are now available via **Help | Manuals | Tutorials**.
140. The **class training materials** are now available via **Help | Manuals | Topics**. These are in the form of PDF files and they are divided into convenient sections. They can be modified by the user or by a class instructor, and supplementary ones can be added. See the *WinSPEED* manual.
141. **Tagged Parameters** have been added in the **template editor** and the **outline editor**. These are intended to assist in training classes and in the navigation and classification of parameters, by use of colour-codes. See the *WinSPEED* manual and *SPEED Dispatches* No. 43.
142. **Replace X_R with XET** has been added in the **template editor** menu. If you have adjusted **X_R** to force *PC-BDC*'s resistance calculation to agree with a measured value, the copper weight **Wt_Cu** will not be consistent with the resistance. Adjustments to resistance should be made by adjusting the mean turn length using **XET**. This function in the template editor automatically calculates the correct **XET** to restore your adjusted resistance value, while resetting **X_R** to 1. The copper weight **Wt_Cu** will change to the correct value, next time you run an **Analysis** calculation. (**X_R** should be used only for "what if?"-type investigations when you are only interested in the effect of resistance variations on the calculated performance).

143. Plotting of the phasor diagram has been corrected for **Connex** = Delta. The phasor diagram titles show "**RMS/ph**" meaning "RMS fundamental phase values". When **Connex** = Delta, the phasor diagram titles show "**RMS/ph eqY**" meaning "RMS fundamental phase values, equivalent WYE".
144. In the phasor diagram, the label "**Vt**" has been changed to "**Vtph**" to agree with the parameter **Vtph** in section 6 (performance) in the DESIGN SHEET.
145. In the phasor diagram, the label "**ZI1**" has been changed to "**VZac**" to agree with the parameter **VZac** in section 6 (performance) in the DESIGN SHEET.
146. **VZac**, **phVZac**, **Vtph**, **VtLL**, **RI1**, **jXdId1**, **jXqIq1**, **Psi_1**, **Psiad1**, **Psiaq1** have been added in the DESIGN SHEET, section 6, to match various quantities found in the phasor diagram and to assist in manual calculations.
147. **[Ctrl+Shift+U]** invokes a user-defined page in the TEMPLATE EDITOR.
148. **[Ctrl+Shift+H]** from the main menu invokes a file history manager.
149. **[Ctrl+Shift+J]** in the GDF editor invokes a list of areas calculated for all sub-regions.
150. In the **Analysis | Ranging** dialog, individual parameters can be cleared using the "Clear" button, instead of clearing all the ranging parameters.
151. **Experimental dials have been added as a display utility.**
152. **Tools|FE Results|MatchFE** now has separate options for **Bgap**, **Btooth**, etc., so that the **Bgap** and **Btooth** windows can be opened with short-cut keys **[Ctrl+Shift+G]**, **[Ctrl+Shift+T]** etc., and can be open at the same time. This makes it easier to coordinate any adjustments made in the B_{gap} and B_{tooth} calculations.
153. The roles of **XBtpk** and **XTTarc** have been changed if **CalcVer** > cv8, making it easier to adjust the B_{gap} and B_{tooth} **GoFERS** independently: this improves the calculation of EMF with **EMFCalc** = ToothFlux when the slots/pole is small (1.5 or less), and makes it easier to get **Eq1** and **PhiM1** consistent with the EMF waveform. See **Eq1tfw**.
154. A new **Tutorial B08** describes the use of the B_{gap} and B_{tooth} **GoFERS** and includes a detailed explanation of the principles of EMF calculation. See also **Tutorial B16** for **generators**, which has been extended with further examples of EMF calculation.
155. The manual has been extended with much more detailed explanation of parameters relating to the advanced current regulators SynchReg and SVMModX, and also relating to the use of variable **Dwell** with squarewave drives.
156. Improvements have been made in the transfer of data to *Motor-CAD*, the thermal analysis program of Motor Design Ltd.
157. The linearized inductance calculation (using frozen permeabilities) has been reinstated in the *i-psi* **GoFER**.

158. In the i-psi **GoFER** options, the label "Inductance" has been made more explicit : "Incremental inductance", to emphasize the fact that this option produces inductance values with frozen permeabilities.
159. The i-psi GoFER can now run with "wild-frequency" harmonic components of current, using parameters **n_W1**, **h_W1**, **ph_W1**, **n_W2**, **h_W2**, and **ph_W2**.
160. Fixed non-repetition of **GoFER** results with exterior-rotor machines when **Shim** > 0.
161. The "Suggested values" of adjustment parameters in the **MatchFE** window of the ipsi **GoFER** previously assumed wye connection, but they now work for delta as well.

PC-AXM — AXIAL-FLUX MACHINES

162. *PC-AXM* is a completely new program for axial-flux machines with several different configurations, including **disk-type rotors** with **slotted**, **slotless**, **airgap**, and **gramme-ring windings** and others. *PC-AXM* also has a model for **claw-pole machines** and two types of **ring-arc (double-airgap)** machines.

PC-IMD — INDUCTION MACHINES

163. A direct solution method has been introduced to simulate steady-state operation based on a matrix analysis of the machine impedances, starting with a primitive impedance matrix and using connection matrices to apply the connections between coils. The calculation is executed using **Analysis | Dynamic design with Drive = Direct**. This technique is designed to include the effects of all MMF harmonics of both the stator and the rotor windings, in a direct simulation of steady-state operation.
164. **AuxSP** has been expanded to give more options for the position of the auxiliary winding in the slot.
165. An additional new method for calculating stray-load loss has been added : **SLLCalc = SEM**. See **SEM-3**.
166. **NRSO** has been added to permit adjustments to Norman's method for leakage saturation.
167. The parameter names in the Hot16 model have been rationalized so that **_1** refers to the drive end and **_2** to the non-drive end, while the subscripts **_DE** and **_ODE** have been eliminated.
168. In the **outline editor**, **Scale dimensions** is a new function that permits the machine to be scaled in the radial or axial dimension. This provides a quick and efficient means of scaling, which is one of the recommended ways of developing new designs from older ones.
169. Also in the outline editor, **[Ctrl+C]** copies the graphical data to a metafile which can be pasted into certain other graphical programs (such as Corel Presentations®) by means of the **Edit | Paste special** function. This gives a far better quality copy than a bitmap image.
170. Graph data can be copied in a form suitable for pasting into a spreadsheet. See the *WinSPEED* manual for this and other interface improvements.
171. It is now possible to disable the sneaky Auto-scale function in graph windows — that's the beastly thing that re-scales the graphs every time you change something, which makes it impossible to see the effect of changes in their true light and proportion.
172. The slider in the **Winding editor** MMF page works. Try it with **Phase = 1** and **Phase = All**, and **Harmonic = 1,2,3** etc.
173. More precise normalization of the MMF and Harmonics has been applied in the **Winding editor**. The mathematics is written up in **SEM-3**, but for a slightly simpler (and more original) account, see [5].
174. The Gorges diagram has an eye to help interpret the phase sequence.
175. Further re-ordering of the **template editor** should help users to navigate the large number of parameters.
176. Some parameter names relating to wire specification have been changed to achieve better uniformity (e.g., **Wire_1**, **Wire_2**, **Wire_A**).

177. *PC-IMD*'s support for the Scott T-connection has been improved with a special version of the phasor diagram.
178. **W_Brg** had no effect on the shaft torque; this has been fixed.
179. Tutorials and Training Class Topics have been added to the Help | Manuals menu. See the *WinSPEED* manual for details.
180. Tagged Parameters have been added to the Template editor and the Outline editor. See the *WinSPEED* manual for details.
181. A program failure when running with **Slip** > 1 and **CanStyle** = Rotor or Both has been corrected.
182. A spurious dip in the torque/speed curve could be obtained with **CanStyle** = Stator or Both. This has been fixed; the previous calculation can be recovered using **RvtWScan** = true.
183. Several errors in the handling of **WIron** and the power balance were obtained with split-phase motors. The most serious is that if **Connex** = SplitPh, **Calc1ph** = XField, and **TapType** = Base, G-tap, or T-Conn, the iron losses were being multiplied by 2 (or nearly 2). If **RvtTap** = FALSE, this error is corrected. The complete set of corrections is described under **RvtTap**.
184. If **IncHx** > 1 and **TapType** = None, the iron loss is not included in the equivalent circuit: as a result the power balance is not observed (i.e., **Pelec** ≠ **Pshaft** + **WTotal**) unless **XFe** = 0. This is an inherent limitation of the method (which is derived from Ref. [36]). A more precise calculation is obtained by setting **TapType** = Base and **Tap** = 0; this calculation is based on **SEM-3** and does not use Ref. [36].
185. If **IncHx** > 1 and **TapType** ≠ None, a divide-by-zero error could occur when one of the harmonic winding factors **kw3**, **kw5**, etc. was zero. This has been fixed.
186. Magnetic wedges have been added for the stator.
187. A divide-by-zero error could occur with certain high-skew motors in calculating the winding factor for the $(S/P \pm 1)^{\text{th}}$ stator slot harmonic, where *S* is the number of stator slots and *P* is the number of pole-pairs. (See Alger, Ref. [3], p. 336, eqn. 9.9).
188. The airgap area **Ag** at the (middle of the airgap) is now calculated for all machines. Previously it was only calculated when **DiffLeak** = CGV.
189. When **RcLoc** was set to AllVolts or AllFlux, **Ic** and **Imc** were not being correctly updated. The symptom of this problem was that **Rc** × **Ic** would be equal to **Xm** × **Imag** regardless of the value of **RcLoc**.
190. The methods for calculating saturation of leakage reactance are described in much more detail (**LkSat**); see p. 97ff.
191. When **LkSat** = Norman and **NeqnR** = N0, **Erb** was previously given in the **design sheet** as zero. This has been changed so that it appears with its original value, in common with the other methods **NeqnR**; method N0 uses **Erb** in a similar way to all the other methods.

192. When **LkSat** = Norman, **NeqnR** = N6,N7,N8 or N9, with closed rotor slots **XkX2slot** was being applied twice. This has been fixed. Datafiles saved with versions compiled before 16-Jan-09 will be automatically updated with a corrected value of **XkX2slot** that produces the same output; but these files must be saved with the new version to retain the corrected value. (Note that **Erb** is set to zero when **LkSat** = SPEED).
193. **SatX1X2** has been introduced to allow the use of saturated leakage reactances in split-phase motors; see p. 99.
194. The manual has a more detailed discussion of the different methods for calculating split-phase and single-phase motors : see p. 100 and Fig. 49.
195. An error in the conversion of conductivity units to resistivity units has been fixed. For example, suppose **PC1** = 50%. If the units are changed to [ohm-m] using [**Ctrl+U**], the result would appear as 8.62E-9 ohm-m, which is incorrect; the value should be $4 \times 8.62E-9$ ohm-m. The performance calculations would remain unaffected as a result of the unit conversion; but if **PC1** (in ohm-m) is now changed to 3.44E-8 in the **template editor**, the results will be incorrect. The error does not arise in converting between conductivity and percentage conductivity; but only between conductivity and resistivity.
196. A check has been introduced for **Rim** = 0 with Type B end-rings.
197. When **Connex** = 3-ph Delt, the equivalent line-neutral reactances **X1_eqy** and **X2_eqy** were derived from the *unsaturated* reactances as **X1unsat**/3 and **X2unsat**/3. They have been corrected so that now they are derived from the saturated reactances **X1**/3 and **X2**/3.
198. When **DiffLeak** = Alger and **Alzz** = XmHx, the unsaturated primary leakage reactance was displayed with an incorrect value; (it was missing the differential leakage component). This has been fixed. It has no effect on performance calculations.
199. **S-Slot** = PllSlot (open or rectangular stator slot) now has three variants, two of which have wedges.
200. PDF bookmarks added to manual.
201. **TGorSO** added, to allow the tang angle of the stator tooth to be defined relative to a line perpendicular to the stator tooth or the slot.
202. The rectangular rotor slot (**Bar1** = Type2) now has three variants, two of which have wedges; see p. 151.
203. **BarExt** was not being added to the rotor bar length for **ERType1**, **ERType2** = Type D. This has been fixed.
204. Small corrections in the geometry of rotor **Bar1** = Type 0 and Type 5 have been made : see Fig. 108. These can be "undone" by setting **RVT_GB15** = TRUE. For Type 1 the error was at the bottom of the slot, while for Type 5 it was near the top. (The correction first appears in version 4.1.1.78).

205. Significant revisions have been made to the calculation of the effect of saturation on the rotor leakage reactance **X2**.
1. The curve-fitting function for Norman's Fig. 5 ("percent zig-zag" vs. flux-density) has been "faired" to eliminate a slight discontinuity at the onset of saturation. (See **SEM-3**).
 2. The Speed method (formerly **LkSat** = SPEED) has been completely revised and incorporated as an option to be used with Norman's method; (use **NeqnR** = NS). This method permits the complete calculation of saturated rotor slot-leakage permeance for closed rotor slots over a very wide range of voltage and current. Old files (saved with versions before 4.1.1.78) will appear with **LkSat** = Norman and **NeqnR** = NS.
 3. Option Ne0 (**NeqnR** = N0) is no longer active, as it is now considered to be too arbitrary. The option (**NeqnR** = N0) is still valid but it has a null effect.
 4. Boldea's method (**LkSat** = Boldea) has been removed. Old files (saved with versions before 4.1.1.78) will be upgraded with **LkSat** = None.
 5. Formerly *PC-IMD* was always using Norman's method N7 for open rotor slots, regardless of the value of **NeqnR**. In the revised version, N6 or N7 can be selected for open rotor slots, and N8 or N9 for closed rotor slots (as Norman originally intended). Method NS, however, can be used with open or closed rotor slots; it can also be used with open slots that are treated as closed by setting **muPlug** = 0.
206. Several minor corrections have been made for the case **MConfig** = ExtRotor, mainly affecting the values of **Wt_AI** and **RotJ**. Some changes will also be seen in the values of the equivalent-circuit impedances, and therefore in the performance.
207. The calculation of **RotJ** has been extended to give more accurate results for all the different types of end-ring. The value of **Wt_AI** will also be affected in come cases.
208. Several small improvements have been made in the calculation of split-phase machines to correct small discrepancies in the power balance.
209. **Bifilar** parameter introduced for specifying bifilar part-winding.

PC-WFC — Commutator machines

210. **URXF** is an under-relaxation factor added to improve the convergence of the nonlinear circuit equations. This should make it possible to get convergence at the extreme ends of the torque/speed characteristic, where there were previously problems of convergence. Files created with earlier versions may load with **URXF** = 0. If so, change **URXF** to 0.4. See p. 48.
211. For comparison of *PC-WFC* with static finite-element calculations it is necessary to specify the DC field and armature currents separately, so **CalcMode** has been given an additional option "rqCurrent" (requested current). When **CalcMode** = rqCurrent and **Drive** = DC, the field current is set with **IFx** and the armature current with **IAX**.
212. A new finite-element **GoFER psiC** has been added to calculate the flux-linkage of the field and/or armature windings as the rotor rotates through one electrical revolution. This is important for computing the EMF under load.
213. The Hot5 thermal equivalent circuit has been improved so that the field and armature resistances are automatically updated with temperature. Also, **hTime**, **maxT_C**, and **dT_Cdt** have been added to make the thermal model better suited for motors that run for a very short time compared with the thermal time-constant (for example, power tools).
214. **CalcMode** = rqTorque has been added so that "requested torque" can be an input parameter. Previously only speed could be specified as an input parameter.
215. Corrected error in inertia calculation
216. Field inductance **Lf** did not include **Lf_gap**.
217. Added **GrRatio** (gear ratio), **GrEffcy** (gear efficiency), **TFric0**, **TFric1** (friction torque components).
218. **ComLead** added
219. Added **PC_S** and **PC_R** to adjust the resistivity of the stator and rotor wires.
220. Added **XWire_S** and **XWire_R** to adjust the stator and rotor wire diameter for stretching during winding.
221. Added **fil_SO** and **fil_TG** (fillet and corner radii at the rotor tooth-tip).
222. Added **RotorID** to allow for a sleeve between the rotor lamination and the shaft.
223. **Tools | Export to DXF** rendered operative.
224. **Bm** is no longer required to be set by the user. If **SetBm** = 0, the magnetic circuit is calculated up to 2.2T in the narrowest section of the magnetic circuit. **Bm** is now an output parameter.
225. **xFTG** is no longer required to be set by the user. If **SetxFTG** = 0, the "FTG" curve in Fig. 42 is automatically calculated to make **ImFTG** = **Im**, and **xFTG** is an output parameter.
226. **xFlux** has been replaced by **SetxkSat**, which can be set to zero.

- 227. **LossFe** introduced to allow the iron loss to be taken as an electrical loss or a mechanical loss. Files created with earlier versions may load with **LossFe** = mech, causing a reduction in torque compared with the value computed in earlier versions.
- 228. Waveforms of rotor tooth flux-density B_{rt} and rotor yoke flux-density B_{ry} are now computed in an extended form so that modulation by the AC fundamental-frequency can be displayed and taken into account in computing the rotor iron losses.
- 229. Rotor iron losses can now be calculated using the extended B -waveforms in Fig. 28. A selection of iron-loss methods is provided *via* the new parameter **WFeCalc**, so that earlier and simpler methods can be reverted to if required.
- 230. **XSyo** : adjustment factor for effective magnetic width of stator yoke.
- 231. **XRyo** : adjustment factor for effective magnetic width of rotor yoke.
- 232. **XLsy** adjustment factor for effective magnetic length of stator yoke.
- 233. **XLry** adjustment factor for effective magnetic length of rotor yoke.
- 234. **XTwR** adjustment factor for effective magnetic width of rotor tooth.
- 235. **XTLR** adjustment factor for effective magnetic length of rotor tooth.
- 236. **Xks** was not implemented in the equation on p. 49.
- 237. With **S_Type** = Round, **Npole** can be greater than 2.
- 238. **Is** introduced; see Figs. 2 and 3.
- 239. **BHeight** added (brush height in the radial direction)
- 240. Small errors in the summation of loss components could lead to situations where **PElec** might not be exactly equal to **Pshaft** + **WTotal**. These have been corrected.
- 241. Fixed a bug in which magnetic circuit calculation would fail if **S_Type** = Round and **xCoil** = 1. This error was caused by incorrect computation of the effective magnetic stator yoke length (off coordinates J,R instead of J,H in Fig. 49). As a result, results for all motors with **S_Type** = Round will change, regardless of the value of **xCoil**, especially if the stator yoke is saturated. Results obtained with earlier versions can only be reproduced by adjusting **XLsy** to give the same effective magnetic length. Unfortunately this is an internal parameter and so the adjustment must be made by comparing **BSY**. In cases where **xCoil** = 1, **XLsy** would need to be set to a very small value (not zero, because *PC-WFC* will only use a positive non-zero value). In upgrading, it is advisable to shelve results with earlier versions and, if necessary, re-calibrate the newer version with any test data.
- 242. Permanent-magnet fields introduced.
- 243. Conductivity units can be changed : use [**Ctrl+U**]
- 244. Introduced temperature-coefficient of conductivity for stator and rotor **TCC_S** and **TCC_R**
- 245. **LossFE** now has a third option : Split

246. Increased the number of segments in the magnetic equivalent circuit model of the stator yoke, from 1 to 3 or 4, depending on the configuration. The flux-density in each section is reported; see **Bsy_1**, **Bsy_2** etc.
247. The mechanical friction torque at the brushes **TBrush** is no longer treated as an input parameter, but is calculated from the brush spring force **FBrush** and the coefficient of friction .
248. Test values **Rf_Test** and **Ra_Test** can be entered as input parameters for comparison with the calculated resistances. Also the temperatures at which they were measured: **TRf_Test** and **TRa_Test**.
249. The torque/speed (or speed/torque) graph has been reformatted with user-definable scales.
250. The **design sheet** is available in tabbed-page format.
251. The **template editor** has new formatting options particularly to make the section headings clearer.
252. **DShxN** and **DShxC** introduced for the diameters of the shaft extensions at the two ends.
253. **MWLspecS** and **MWLspecR** introduced to provide alternative methods of specifying the magnet wire length and resistance. See associated input parameters **kappa_S**, **kappa_R**, **Tkappa_S**, **Tkappa_R**; and output parameters **MWL_S**, **MWL_R**, **kappaS20** and **kappaR20**.
254. **PathEMF** introduced so that the path EMF can be calculated from “point-contact” brushes, or from the fundamental of the graph of path EMF versus brush-shift.
255. **SBshift** introduced so that user can choose whether a positive value of brush-shift (**BShift**) is in the direction of rotation, or against it.
256. **WIQ** > 0 detail modification for lamination geometry for **S_Type** = Square, **DimGroup** = dg1.
257. **Dynamic braking introduced.**
258. **uRXM** introduced as a further means of recovering stability in the solution in very highly saturated cases. In the event of convergence failure, set **URXM** to a lower value (e.g. 0.4 or even 0.1).
259. The effect of armature reaction on the airgap flux-distribution at high values of **BShift** has been corrected. In particular, if **BShift** = 90° or -90°, the previous version was not applying the armature reaction MMF waveform correctly. **BSRevert** = TRUE will revert to the older calculation.
260. The text file WFCCoils.dat is now consistent with the Winding editor, as to coil-side locations in slots, and comm. segs. to which attached.
261. For retrogressive windings the armature-reaction "tips" the Bgap distribution in the opposite way, compared with progressive windings. In both cases the leading edge has the higher flux-density, but the direction of rotation is opposite in the two cases. There is no significant effect on results unless **Throw** is abnormally small.
262. **BShift** and **ComLead** now treated the same with respect to **XBShift**.

- 263. Added separate adjustment factors for rotor and stator iron losses, **XFeR** and **XFeS**.
- 264. Corrected an error in the displayed phase angle **phVt**, which was too large by a factor $180/\pi$.
- 265. Introduced **rqPelec** and **rqPshaft** as inputs with **CalcMode**, so that the operating point can be specified in terms of required electrical power input or required mechanical power output.
- 266. Modified the lamination detail around the *d*-axis and the *q*-axis, to give more flexibility with tabs and cut-outs. See Fig. 48 on p. 93. Also see name changes for **RNq**, **WID**, **RND**, **DND** in the next section. Added new parameters **FIQ**, **FOQ**, **FOD** to be used with the detail of tabs and cut-outs.
- 267. Added a graph of EMF vs. field current E(I_f)OC; this is the "DC test" value of armature EMF with zero current in the armature; see Fig. 23 on p. 21. Introduced **EIGraphs** (selects EI graphs for display).
- 268. Corrected the value of G(β) when **G_beta** = None; previously it was being set equal to 1, but the correct value is 0. The effect of the error was that the *d*-axis component of armature-reaction MMF was being applied with 100% of its value for all values of **BShift** (or **ComLead**), including zero.
- 269. Added a calculation of the AC locked-rotor test with the armature open-circuited; see p. 82.
- 270. Added **SComLead** and **Rotation**, with arrow in the **winding editor** indicating direction of rotation.
- 271. Added directional arrows in the winding editor to show the direction of current flowing in conductors.
- 272. Extensive modifications to torque/speed graphs and related graphs, giving much improved control of the display. Also added an overlay facility to display previously-saved graphs.
- 273. Revised manual with re-ordering of sub-sections in Input parameters (section 3.2).
- 274. Errors in **ASBlank**
- 275. Introduced **TC_R2**, **TC_R3**, **TC_R4** to allow different numbers of turns in groups of armature coils.
- 276. Introduced **Rspec_S** and **Rspec_R** so that the calculation can be forced to use the test values of field resistance (**Rf_Test**) and armature resistance (**Ra_Test**) to be used in the performance calculation.
- 277. Correction : the effect of **XWire_R** on **kappaR20** was missing. (Relevant only when **MWLspecR** = MLT or TWL). The armature resistance will be affected in cases where **XWire_R** is non-zero.
- 278. Correction : the effect of **XWire_S** on **kappaS20** was incorrectly formulated. (Relevant only when **MWLspecS** = MLT or TWL). The field resistance will be affected in cases where **XWire_S** is non-zero.

- 279. Correction : errors in the formulation of the reactances **Xmd** and **Xmd0** and the *d*-axis permeance **Pmd0** have been corrected. To see the effect, use the reversion switch **Pmd0_Rvt**.
- 280. Introduced automatic calculation of the locked-rotor condition when **CalcLR** = true.
- 281. Introduced automatic calculation of the no-load condition when **CalcNL** = true
- 282. Introduced automatic calculation of the range of the torque/speed characteristic if **TSrange** = Auto.
- 283. Introduced **thm_dt** with a default value of 0.1 sec, to stabilize the Hot5 model in cases requiring a small thermal integration time-step. The previous fixed default value of this time-step was 1.0 sec.
- 284. Corrected the criterion that stops the Hot5 model when the rate of change of temperature at the C node exceeds **TC_rate**. If this rate of change was negative, the calculation would stop prematurely.
- 285. **ThR_G** was not available in the template editor, and previously it had a default value of 1 °C/W. Now if **ThR_G** = 0, *PC-WFC* calculates the thermal resistance across the airgap automatically. See also **HTC_g**.
- 286. Introduced Hot5 graphs of temperature vs. time.
- 287. Introduced **NomTshNL** and **NomRPMNL** to give better control of the no-load calculation.
- 288. Introduced **CvgNL** and **CountNL** to monitor the convergence of the no-load calculation.
- 289. Introduced **Tol** to give user control of the convergence tolerance used in circuit simulation.
- 290. Introduced **UseEICS** to give an optional faster solution algorithm for DC motors.
- 291. **New Tutorial W01** describes the basic operation of *PC-WFC* for all the basic motor types, DC and AC, wound-field and PM.
- 292. Several new **standard examples** are available with **File|New** (or by using the short-cut keys [**Alt+1**], [**Alt+2**] etc.)
- 293. Further reorganization of the **template editor**, which now has three pages and better segregation of different types of parameters.
- 294. Many new features and improvements in the interface are described in the *WinSPEED* manual: for example, **Graph|Save graph data**, Graph options [**F8**], 3d view using **OpenGL 3d** (p. 11), **DXF overlay** (p. 12), **Scale Dimensions**, (p. 10).
- 295. Added **Xrm** to adjust the radius of the arc at which the magnet width is calculated in PM stator types.
- 296. Added **FMOH**, the factor by which the flux/pole is increased when the axial length of the magnet exceeds the armature length; ("magnet overhang").
- 297. Added **A_sp**, **L_sp** and about 10 other areas and lengths defining sections of the magnetic equivalent circuit.

298. Significant changes have been made in the circuit solver for DC motors (**Drive** = DC), to ensure that the current used in calculating the armature reaction is correctly calculated and updated at the operating point. Results from previous versions should be checked, and any problems reported to the *SPEED* Laboratory.
299. Improvements have been made in the no-load calculation and it is now recommended to use **CalcNL** = true and **CalcLR** = true in most cases, as a safeguard against trying to calculate outside the normal motoring range.
300. Corrections and improvements have been made in the automatic calculation of performance curves when **CalcMode** = rqCurrent, rqPower, etc., although the fastest and simplest way is still with rqRPM.
301. Significant improvements in the speed and stability of the circuit solvers have been achieved so that it is now generally possible to run with **URXF** = 1. The improvement in speed of calculation should be noticeable — in some cases as much as a factor of 6 times.
302. An error in the calculation of **La_gap** has been corrected. Although this parameter has almost no significance in performance calculations, the difference between new and old values will be found equal to the number of parallel paths. See **Lgap_Rvt**.
303. The options available with **EMFCalc** have been extended so that the EMF can be calculated by formula from the flux/pole, instead of by the "waveform" technique. This may give better accuracy in some cases.
304. **ShAxFlux** has been introduced to allow for the axial spreading of flux in the frame. This also produces a modification in the frame shape in the finite-element GoFER.
305. The standard example menu (**File|New**) has been revised, to give a wider range of options, and the standard example PM motor has been changed to use the same rotor as all the other examples.
306. Further improvements have been made in the torque/speed graph format, including the provision of points [P] and the annunciation of the cursor coordinates corresponding to points on each curve. Torque/speed graphs can now show negative current and torque for DC motors.
307. **SatXm** introduced to provide an alternative method of calculating the saturation of **Xmd** and **Xmq**.
308. Further improvements have been made in the calculation of no-load speed, including 3 optional methods that can be selected using **CalcNL**; also, **TSrange** and **CalcLR** have been removed. See p. 41.
309. A problem with the resetting of **IAX** has been fixed.
310. An error has been fixed in the application of the armature-reaction MMF distribution for **NPole** > 2.
311. Several parameters from section 6 of the **design sheet** ("Magnetic Circuit") have been removed to a new section "10. Program Control and Magnetic Circuit Adjustment" in order to simplify the sections of the **design sheet** that are of most interest.

312. The **Winding editor** has been improved. It now has an automatic calculation [**F9**] which highlights one electrical path. This is in addition to the existing "Highlight Path" function, which carries the highlighted coils along with the armature and does not recognize the effect of commutation. The new function not only recognizes the function of commutation but also shows a shorting link near the brushes when they are shorting the tails of a coil undergoing commutation. The new **Winding Editor** also has arrows for current in active paths, and EMF in conductors passing the poles.
313. Tutorials and Training Class Topics have been added to the Help | Manuals menu. See the *WinSPEED* manual for details.
314. Tagged Parameters have been added to the **Template Editor** and the **Outline Editor**. See the *WinSPEED* manual for details.
315. An error in the conversion of conductivity units to resistivity units has been fixed. For example, suppose **PC_S** = 50%. If the units are changed to [ohm-m] using [**Ctrl+U**], the result would appear as 8.62E-9 ohm-m, which is incorrect; the value should be $4 \times 8.62E-9$ ohm-m. The performance calculations would remain unaffected as a result of the unit conversion; but if **PC_S** (in ohm-m) is now changed to 3.44E-8 in the **template editor**, the results will be incorrect. The error does not arise in converting between conductivity and percentage conductivity; but only between conductivity and resistivity.
316. **thm_dt** restored in the template editor, with default value increased from 0.1 to 1.0s.
317. Corrections to Hot5 thermal model. The rate-of-temperature-rise criterion has been disabled because it could cause premature termination of the transient thermal calculation.
318. Corrections to the display and calculation with Rotation, Bshift, SBshift, ComLead and SComLead.
319. Several improvements in the manual, including explanations of EMF parameters and Flux parameters.
320. **PhiGwfm** removed. ("Airgap flux per pole calculated by integrating the absolute value of the airgap flux-density distribution over 360°, dividing by 360°, and multiplying by the airgap area per pole.") **EPphi** is now calculated from **PhiGmct**.
321. Added **EffGap** in the design sheet.
322. Revised the calculation of **Pmd0** and **Pmq0**. Results depending on inductance will change slightly.
323. Complete revision of the assignment of ampere-conductors to the slots for the **PsiC GoFER**. Results will change. This eliminates a persistent problem with a spurious phase-shift in the comparison between *PC-WFC* and *PC-FEA* in the **MatchFE** for the **PsiC GoFER**.
324. The parameters in the **Winding editor** have been rearranged in a more logical fashion, so that **Rotation**, **Ashift**, **SComLead**, **ComLead**, **SBshift** and **Bshift** are grouped together.

- 325. The Coil List has been revised to correct a problem with the assignment of currents in the ampere-conductor assignment in the GoFER when **ProgRet** = Retro. (The Coil List is available in the text file WFCCoils.dat after **Analysis | Static design**).
- 326. Slot numbers have been added in the **Outline Editor** and the **Winding Editor**.
- 327. **mica** is now displayed in the **Winding Editor**. It is also incorporated in the calculation of brush contact area.
- 328. When **EMFCalc** = IntBgap, the EMF, **kT** and **kE** were not changing when **Plex** was changed from Simplex to Duplex or Triplex, even though PathsR was changing correctly. This is fixed.
- 329. Fixed the discontinuity in the return coil-side in the winding-editor display when **Skew** \neq 0. This error was introduced in 2010. It had no effect on the performance calculation.
- 330. Introduced **rqI_Mode** to give an additional option Fix_RPM for calculating with **CalcMode** = rqCurrent.
- 331. Introduced **RPM_init** to give a choice of starting values of RPM in iterative calculations with **CalcMode** = rqTorque, rqCurrent, etc.
- 332. Introduced **URXY** to give control of the under-relaxation factor used in iterative calculations for the speed.
- 333. Some versions had an option **CalcNL** = SkipNL. This has been disabled. Use **CalcNL** = NomRPMNL instead.

PC-SRD — SWITCHED RELUCTANCE MACHINES

- 334. The **[F11]** finite-element **GoFER** has been updated with several new features taking full advantage of the latest version of *PC-FEA* (5.5), including
 - 1. the ability to calculate with multiple phases conducting simultaneously;
 - 2. ideal current waveforms, or dynamic current waveforms calculated by *PC-SRD*;
 - 3. display of the finite-element *i*-psi loop superimposed on *PC-SRD*'s loop
 - 4. special viewer for analysing the current and flux-linkage waveforms and the resulting *i*-psi loop, with any number of phases conducting simultaneously;
 - 5. automatic addition of end-effects under the user's control;
 - 6. compatibility with *PC-FEA* 5.5; and
 - 7. similar operation to the *i*-psi **GoFER** in PC-BDC.

This upgraded facility makes it possible to study the effect of magnetic interaction between phases far more effectively than was possible before.

- 335. The older **Unimesh GoFER** is retained because of its efficiency in calculating mag. curves and "USA points"; it now has an option to use the original unchanged *PC-FEA* Version 2, or to switch to *PC-FEA* 5.5 which gives better access to the finite-element script and more advanced facilities in meshing and post-processing.
- 336. When **StepGap** = Stepped and **NonSym** = True, **Tools | Realign** was not applying the end-effects with the correct "roll-off" function. This has been fixed, so that external mag. curves can now be used correctly with nonsymmetric motors.
- 337. A serious overestimation of transistor turn-on loss associated with **tq_ON** has been corrected. The output parameter is **ConvLoss**.
- 338. **Tools|Realign mag curves** now expects "additional inductance" terms **dLau** and **dLu** in millihenries, instead of henries.
- 339. [**Ctrl+C**] in graphics windows simultaneously copies data in a numerical format that can be pasted into a spreadsheet.
- 340. Many new features and improvements in the interface are described in the *WinSPEED* manual: for example, **Graph|Save graph data**, Graph options [**F8**], 3d view using **OpenGL 3d**, **DXF overlay**, and **Scale Dimensions** in the **outline editor**.
- 341. Tutorials and Training Course Topics have been added to the Help | Manuals menu. See the *WinSPEED* manual for details.
- 342. Tagged Parameters have been added in the **template editor** and the **outline editor**. See the *WinSPEED* manual for details.